Supplementary Materials for

A flexible multimodal pulse sensor for wearable continuous blood pressure monitoring

Shuo Tian, Liangqi Wang, Rong Zhu*

State Key Laboratory of Precision Measurement Technology and Instrument, Department of Precision Instrument, Tsinghua University, Beijing, 100084, China.

*Corresponding author: Rong Zhu

Email: zr_gloria@mail.tsinghua.edu.cn

Note S1. Fabrication of the flexible sensing layer

The fabrication process of the sensing layer flexible thermal film involves several steps. First, the electrodes and wires are printed on a polyimide substrate (DuPont Pyralux AP8525R) using a flexible printed circuit (FPC) technique. Next, a photoresist is sprayed onto the printed substrate and patterned by photolithography. Then, a film of Cr/Pt (35 nm/100 nm) is deposited continuously by magnetron sputtering and patterned by the lift-off process. The sensors are then annealed in a vacuum furnace at 200°C for 2 hours and cleaned with absolute ethanol and deionised water. Finally, a parylene layer (2 μm) is applied to the sensor using chemical vapour deposition (PDS 2010 Labcoter 2) as an encapsulation. This process results in a flexible thermal film that can measure pressure pulse signals and body surface temperature simultaneously. The fabrication of the interface sensor is shown in the figure below.

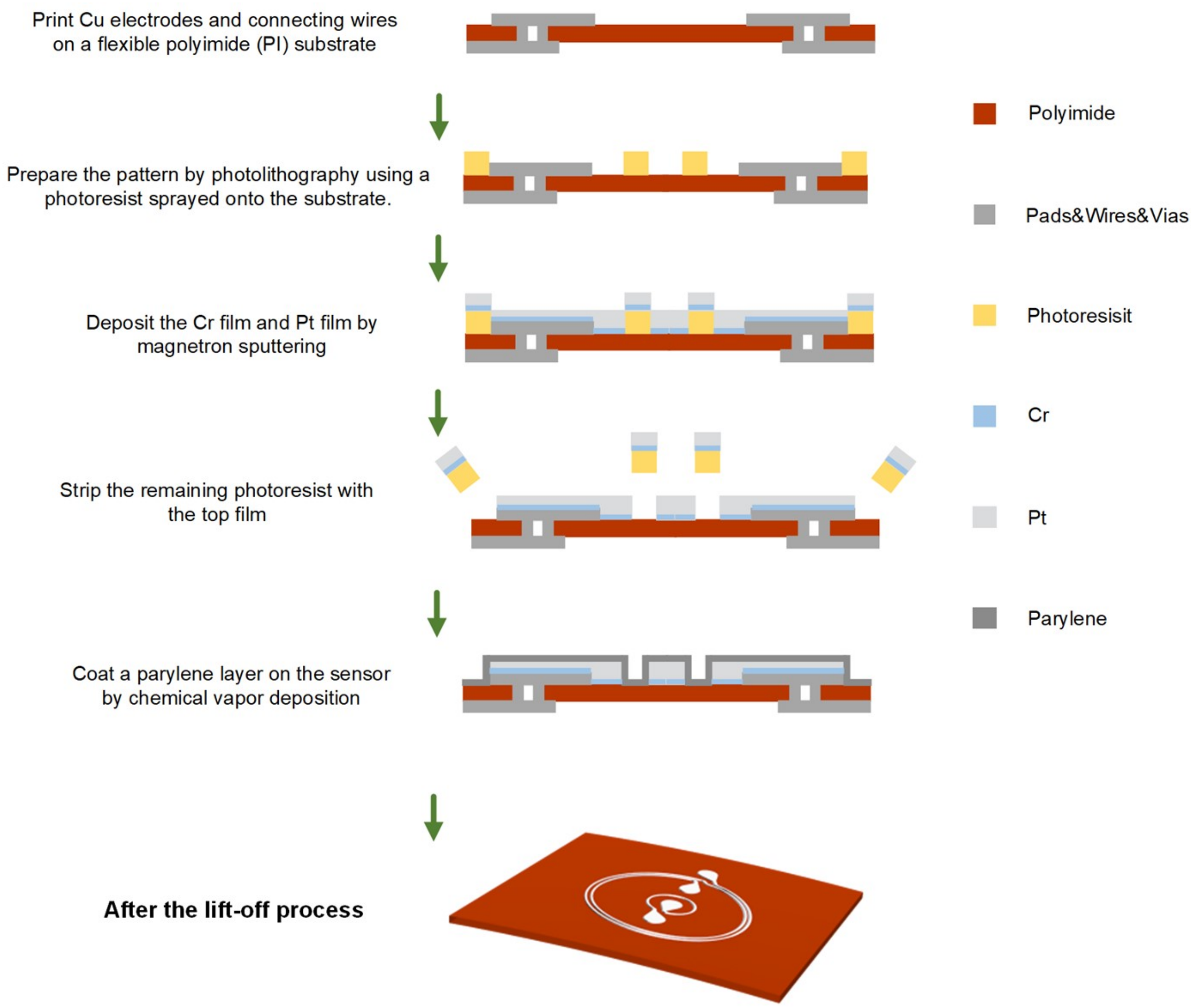

Note S2. Fabrication of the porous silver-particle reinforced PDMS

To prepare the porous PDMS material, a cross-linked PDMS solution (Dow Corning Sylgard 184, 10:1 weight ratio of alkali to cross-linker) was used for the substrate, which was doped with silver nanoparticles at a volume ratio of 2%. After mixing well, a calculated volume fraction of citric acid monohydrate particles is added and stirred well to form a semi-solid mixture. By pouring the mixture into an acrylic sheet mould, heating it in an oven at 80°C for 2.5h and peeling off the mould after solidification, the PDMS is made in square form. The material is placed in an ultrasonic cleaning oven and cleaned with anhydrous ethanol for 1min, followed by a 24h soak in anhydrous ethanol, the surface is washed with water and then dried in an oven at 45°C for 20min to obtain the final PDMS composite pizeo-thermic material for use. The fabrication of the porous silver-particle reinforced PDMS is shown in the figure below.

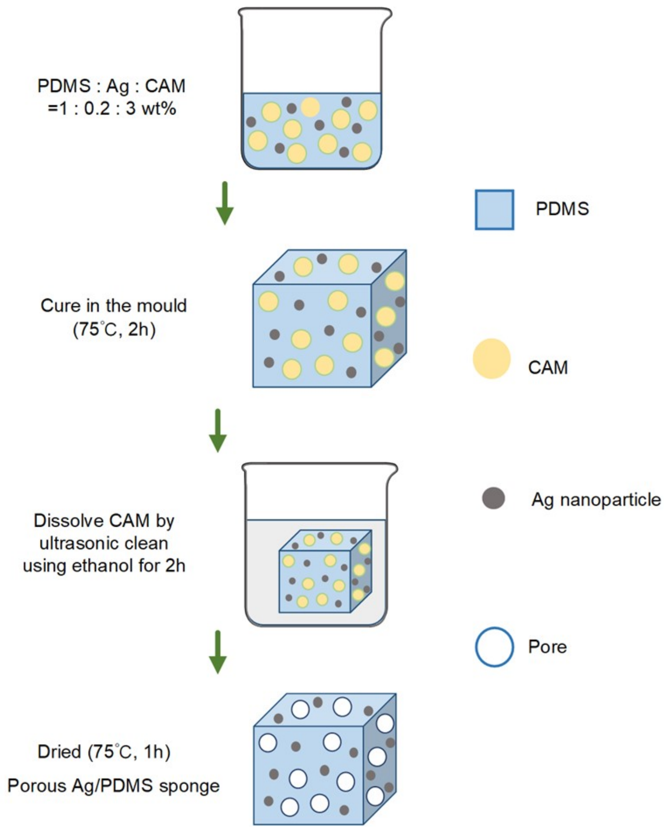

Note S3. The principle of temperature compensation by the CTD scheme

As shown in the figure below, the reasonable resistor configuration of the Wheatstone bridge in the CTD (Constant Temperature Difference) circuit enables effective temperature compensation and decoupling of the bimodal measurements, supporting independent measurements for pressure/temperature or proximity/temperature.

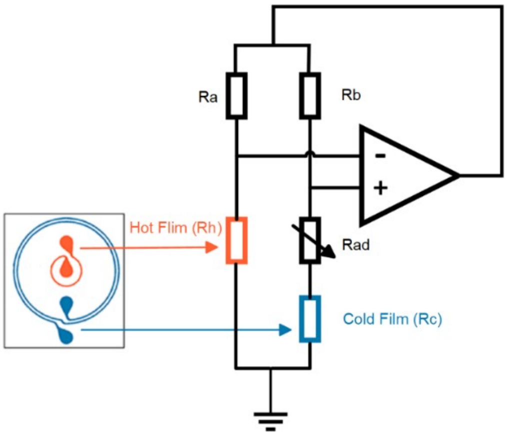

When the Wheatstone bridge is balanced, the relationship of resistors within the bridge can be expressed as follows:

$$R_a \times (R_{ad} + R_c) = R_b \times R_h \tag{1-1}$$

Set the resistance ratio of R_a and R_b as:

$$\frac{R_a}{R_b} = \frac{R_{h0}}{R_{c0}} \tag{1-2}$$

The temperature coefficient resistances (TCR) of the hot and cold films are approximately equal and are denoted as α_h and α_c, respectively. R_{h0} and R_{c0} are the resistances of hot film and cold film at $0\ ^oC$. T is the ambient temperature, ΔT is the temperature difference between the hot-film and the environment. Bringing in the TCRs of the hot film and the cold film, Equation (1-1) can be further derived as follows:

$$R_a \times [R_{ad} + R_{c0}(1 + \alpha_c T)] = R_b \times [R_{h0}(1 + \alpha_h T + \alpha_h \Delta T)] \tag{1-3}$$

From Equations (1-1), (1-2), and (1-3), the resistance configuration of the CTD circuit can be derived as follow:

$$\begin{cases} \dfrac{R_a}{R_b} = \dfrac{R_{h0}}{R_{c0}} \\ \Delta T = \dfrac{R_{ad}}{R_{c0}\alpha_c} \end{cases} \tag{1-4}$$

Equation (1-4) shows that the temperature difference is independent of the ambient temperature. Therefore, the output voltage U_{top} is independent of the ambient temperature.

Note S4. The pressure sensing performance of pulse sensor

The pulse sensor is tested by using a force gauge (Sundoo SH-5, 0.01N resolution). The pressure stimulus is applied by using a mechanized z-axis stage (Handpi HLD) with the force gauge. The pulse sensor responds to the pressure stimuli as shown in the following figure, indicating a measuring range of 0-228kPa.

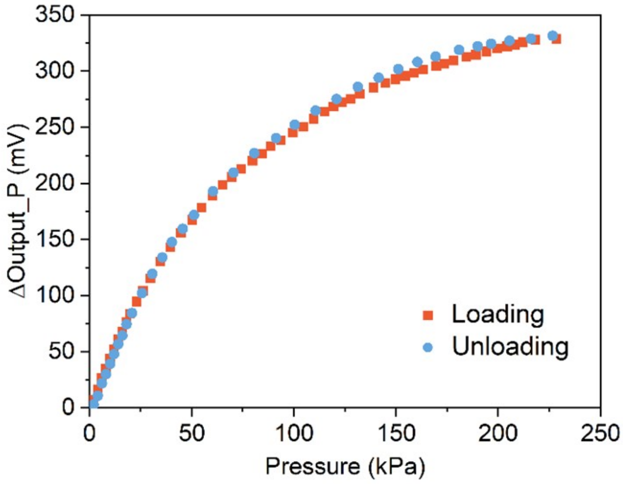

The pressure detection limit is tested by placing a tiny plastic cap nut on the sensor. The following figure shows a weight of 4 Pa is applied on the sensor. The response of the pulse sensor indicates a low detection limit of 4 Pa.

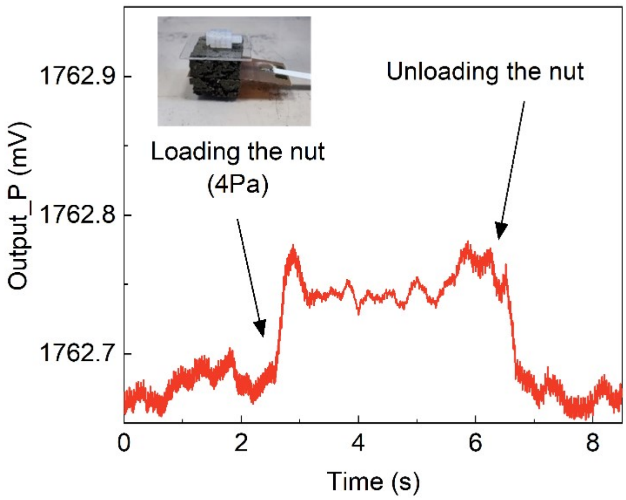

The dynamic response is tested by instantaneously loading a pressure onto the sensor. The response of the pulse sensor is shown in the following figure, indicating a response time of 88ms.

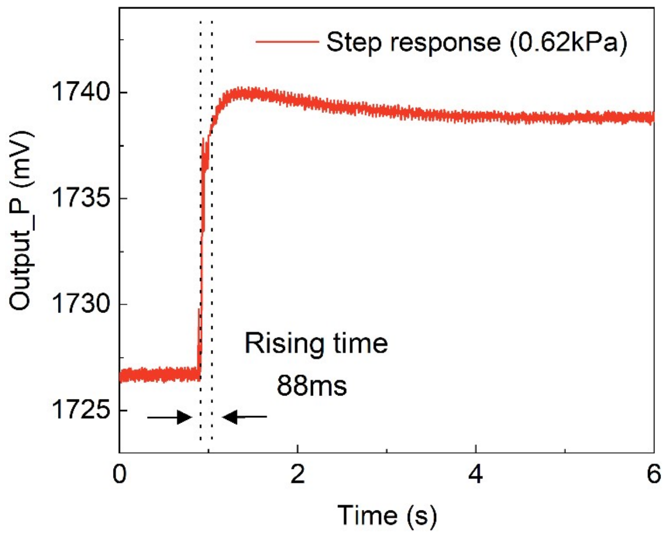

Cyclic pressure loading experiment is conducted by alternately loading the pressure stimuli between 10 and 50 kPa for more than 1000 times. The sensor responses are monitored and shown in the following figure, indicating good durability and stability.

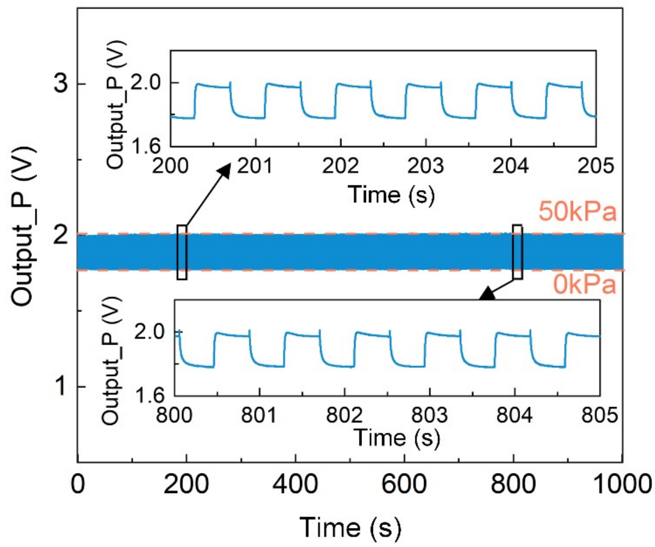

Note S5. The principle of temperature measurement

In our sensor design, the hot and cold films are connected to the two ends of a Wheatstone bridge to realize the Constant Temperature Difference (CTD) mode with the help of a CTD circuit. Since the resistance of the cold film is much larger than that of the hot film, the Joule heat of the cold film is negligible according to the CTD circuit. Therefore, the temperature of the cold film is approximately equal to the ambient temperature. As defined in Supplementary Note S2, α_c is the TCR of cold-film, R_{c0} is the resistances of cold-film at $0\ ^{o}C$, T is the ambient temperature. The cold film resistance with respect to the ambient temperature can be expressed as follows:

$$R_c = R_{c0}(1 + \alpha_c T) \tag{2-1}$$

In the Wheatstone bridge, the voltage ratio of cold-film can be calculated by:

$$Output\_T = \frac{U_+}{U_{top}} = \frac{R_c + R_{ad}}{R_c + R_{ad} +} \tag{2-2}$$

Combining Equation (2-1) and (2-2), there is a linear relationship between ambient temperature T and temperature signal $Output\_T$

$$Output\_T = \frac{R_{c0}}{R_b}\alpha_c T + \frac{R_{ad} + R}{R_b} \tag{2-3}$$

Note S6. Device design

The wearable device is operated by a signal acquisition and transmission circuit, including a sensor conditioning circuit and a digital circuit, where the sensor signals are acquired by a microcontroller unit (MCU: STM32L452) via an analog-to-digital converter (ADS124S06) and wirelessly transmitted to an external terminal (e.g. PC or cellphone) via a low-power Bluetooth module (DA14580). The sampling frequency of the sensor is 125 Hz. In addition, a non-essential PPG sensor with a sampling frequency of 1000 Hz was used to monitor the pulse signal at the fingertip and was used as a comparison at follow-up. The PPG sensor is a reflectance type (MAX30101, Maxim) with a photodetector and a 525 nm (green) LED. The device case is made of resin and 3D printed. A lithium-ion battery is used for the power supply and can be charged through the Micro-B USB connector plug.

Note S7. The detailed process of pulse signal processing

First, we remove the outliers of the pulse signal and high frequency noise. The outliers of the original pulse signal are detected and replaced with linearization by a window of length 20 points and the 3σ principle. Then, a window of length 3 is applied to smooth the pulse signal to obtain a clear pulse waveform. Next, a Savitzky-Golay filter with a window of the signal length and polynomial order = 4 is applied to obtain the baseline. The baseline is subtracted from the clear pulse waveform and the average of the baseline is added to obtain the pulse waveform with the baseline removed.

Note S8. Definition of the features extracted from the pulse signal

The 33 features extracted from pulse signal and subject information are defined as the following table. Pm is the mean value of the pulse wave signal, Pd is the mean value of two valleys, and Ps is the peak value. K value in a cardiac cycle is calculated by (Pm-Pd)/(Ps-Pd). The bigger the K value is, the smoother the waveform is.

Type of parameter	Featues	Definitions
Pulse waveform features	Pd	Value of minimum pressure
	Ps	Value of percussion wave
	Pdn	Value of dicrotic notch
	Pdw	Value of dicrotic wave
	Ppp	Peak-to-peak value of the pulse wave signal
	PIR	Ratio of pulse signal peak to foot amplitude
	PR	Pulse rate
	T	Cardiac period
	ST	Systolic time
	T-AE	Time span between point A and point E
	T-BE	Time span between point B and point E
	T-CF	Time span between point C and point F
	RtTP	Time ratio of TCD to cardiac period
	K	Pulse wave signal characteristic value
	K1	Systolic characteristic value
	K2	Diastolic characteristic value
	AS	Ascending slope of pulse signal
	K1/K	Ratio of K1 to K
	K2/K	Ratio of K2 to K
	dPW_PAm	Peak amplitude of first-order difference of pulse signals

	dPW_TW	Time wide of first-order difference of pulse signals
	dPW_AS	Ascending slope of first-order difference of pulse signals
	dPW_DS	Descending slope of first-order difference of pulse signals
Wearing pressure and skin temperature features	Temp	Skin Temperature
	Pm	Baseline value of the pulse wave signal
	Fre1	Amplitude at the pulse rate
	Fre2	Amplitude at the 1st harmonics
	Fre1-T	Amplitude of the temperature signal at the 1st harmonics
Physical characteristics	Age	Height of the subject
	Height	Age of the subject
	Weight	Weight of the subject
	Gender	Gender of the subject
	BMI	Body mass index of the subject

Note S9. The optimization process of the MLP neural network

In the optimization process of the MLP neural network, pulse waveform features, wearing pressure, and skin temperature features, and the subject's physical characteristics are used to estimate SBP. To avoid overfitting, a penalty term (L2 regularization) is added to the loss function to perform weight attenuation and limit the sum of squares of the neuron weights. If the error of the validation set does not decrease after several rounds of training, the training is stopped, and the trained model is used as the model of the sensor.

The number of layers, the number of neurons and Dropout of the hidden layer of the neural network are optimized, and the results are shown in the table below. When the number of hidden layers is 1, with the increase of the number of neurons, the absolute value of the average error of systolic blood pressure and the standard deviation of the error are reduced. With the increase of the number of neurons, the average error and standard deviation gradually decrease and tend to be stable. The estimation accuracy of the double hidden layer structure is improved compared to the single hidden layer structure. Therefore, the best MLP structure is a double hidden layer structure, the first hidden layer is 80 neurons, and the second hidden layer is 20 neurons. A Dropout of 10% is applied to each hidden layer. This neural network will be used later to estimate systolic and diastolic blood pressure.

neural network structure*	error (ME±SD)	neural network structure	error (ME±SD)
12	0.62 ± 6.75	30+30	0.65 ± 6.08
20	0.16 ± 6.21	30(0.1)+30(0.1)	0.42 ± 6.04
30	-0.08 ± 5.95	40(0.1)+40(0.1)	0.22 ± 5.82
50	-0.16 ± 5.90	50(0.1)+50(0.1)	0.49 ± 5.78
80	-0.14 ± 5.89	80(0.1)+50(0.1)	-0.70 ± 5.67
100	0.33 ± 5.87	80(0.1)+20(0.1)	-0.03 ± 5.56
100 (0.1)	0.62 ± 5.83	80(0.2)+20(0.2)	0.70 ± 5.76

*：The number is the number of neurons in the hidden layer, and the number in parentheses is the Dropout ratio

Note S10. Details of blood pressure measurement

There are a total of 18 subjects, 13 males and 5 females. The measurement time of each subject is about 1 minute each time, and the measurement interval is at least 3 minutes. Each person measures at least 10times, and the measurement is divided into at least 2 days. The subjects remove and re-wear the our wristwatch device between different measurements to validate the feasibility and generalization across different wears. There are 260 measurements in total. When measuring, the subject wears the device on the left wrist and wears a commercial cuff-based blood pressure monitor (OMRON J751) on the upper arm of the right hand for simultaneous measurement. The blood pressure measured by the cuff-based blood pressure monitor is used as a ground truth blood pressure. The data were distributed as follows.

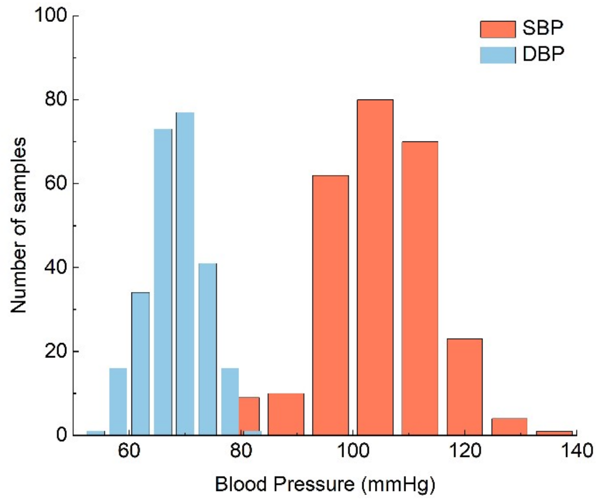

Note S11. Performance metrics

Mean error (ME) is the average of the errors of all estimates and reference values. Let there be a total of N pairs of blood pressure estimates BP_{est} and blood pressure reference values BP_{ref}, the mean error is defined as:

$$ME = \frac{1}{N}\sum_{i=1}^{N}(BP_{ref,i} - BP_{est,i})$$

The standard deviation (SD) can be a measure of the dispersion of a set of data and is defined as:

$$SD = \sqrt{\frac{1}{N}\sum_{i=1}^{N}\left(BP_{ref,i} - BP_{est,i} - ME\right)^2}$$

The Mean Absolute Error (MAE) represents the mean absolute error between the predicted and observed values and is defined as:

$$MAE = \frac{1}{N}\sum_{i=1}^{N}|BP_{ref,i} - BP_{est,i}|$$

The Pearson correlation coefficient is used to measure the linear correlation between two sets of data and in this paper it is calculated as：

$$r = \frac{\sum_{i=1}^{N}\left(BP_{est,i} - B\bar{P}_{est}\right)\left(BP_{est,i} - B\bar{P}_{est}\right)}{\sqrt{\sum_{i=1}^{N}\left(BP_{est,i} - B\bar{P}_{est}\right)^2}\sqrt{\sum_{i=1}^{N}\left(BP_{ref,i} - B\bar{P}_{ref}\right)^2}}$$

Note S12. Details of the neural network for PWA

The neural network framework of the PWA (PP-net) refers to the framework proposed in the related literature[1]. It is shown in the figure below.

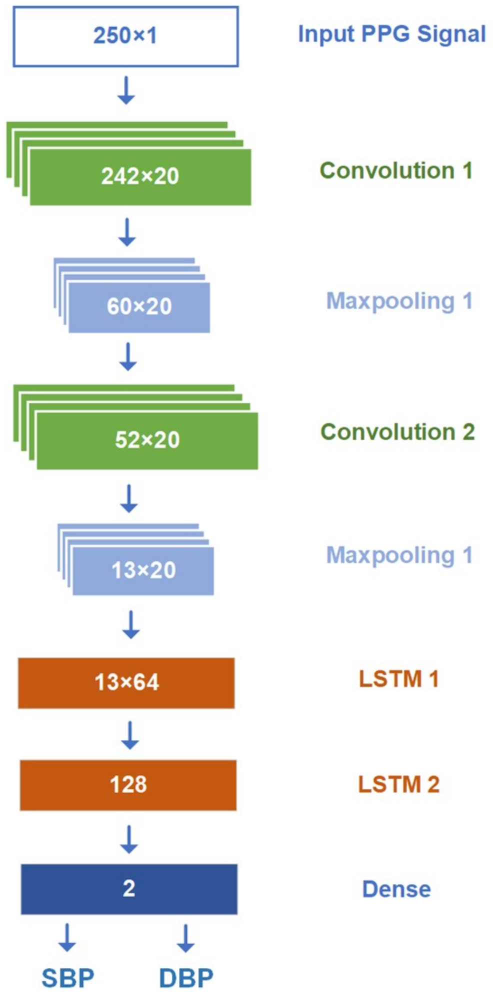

The PWA network takes backlit sphygmomanometer (PPG) waveforms as inputs and provides either systolic blood pressure (SBP) or diastolic blood pressure (DBP) as outputs. It is a hybrid architecture and combines Convolutional Neural Network (CNN), Long Short Term Memory (LSTM) and Dense. Each of the two 1D convolutional layers consists of a set of 20 learnable filters of size 9×1. Subsequently, the spatial dimensions (width, height) are pooled by 4×1 using a maxima operation. Next, two LSTM layers with 64 and 128 storage units, respectively, are combined with a CNN model using hyperbolic tangent for the regression problem. Finally, a fully connected layer with 2 output neurons is introduced to find the final predicted score using a linear function, where DBP, SBP are predicted one by one through each output neuron. A culling layer with a probability coefficient of 0.1 is used after each pooling layer, which forces the network to be redundant and helps mitigate the overfitting problem. The parameters of each hidden layer of the neural network were taken from references to ensure consistent network construction.

Fig. S1. Photograph of blood pressure measurement. The blood pressure of the subjects is measured using our wristwatch device. Our wristwatch device is worn on the left wrist for blood pressure measurement. Simultaneously, a commercial cuff sphygmomanometer (Omron J751) is worn on the right upper arm to conduct the blood pressure measurements synchronously. The blood pressure results measured by the cuff sphygmomanometer are as the reference or ground truth blood pressure for comparison with the measurements using our wristwatch device.

Fig. S2. User interface of the wearable system. The system provides the real-time monitoring on pulse wave, skin temperature, heart rate, and blood pressure.

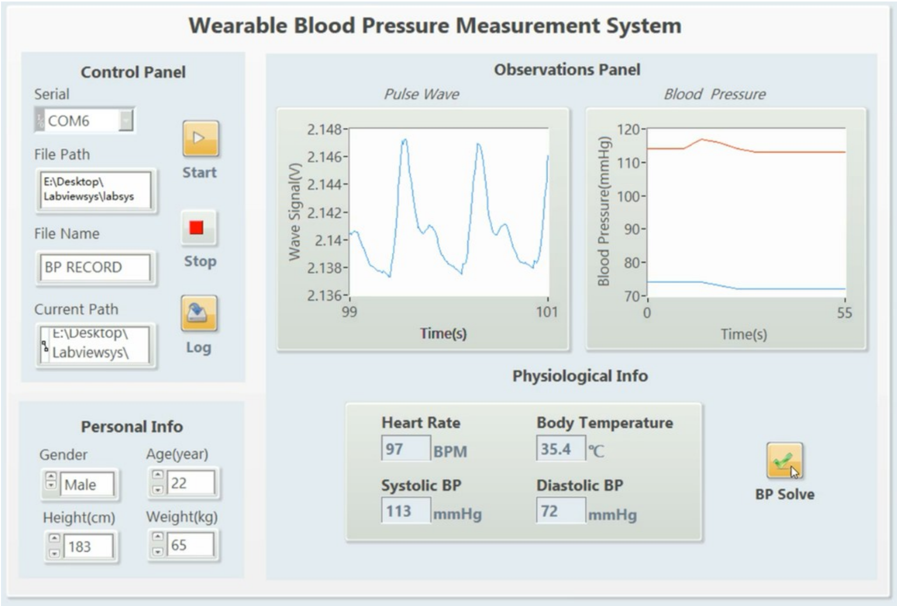

Table S1. The comparisons of different types of pressure sensors

Sensor type	Sensing materials	Output for one pulse wave	Measuring Range	Sensitivity	Linearity	Detection limit	Skin Temperature	Contact pressure	Ref.
Multimodal piezo-thermic sensor	**Skin & Pt**	**0-70 mV (adjustable)**	**0-228.2kPa**	**7.85mV·kPa^{-1} (8-20kPa)**	**0.999**	**4Pa**	**yes**	**yes**	**This work**
Piezoresistive sensors	Polyaniline	△I/I0 0.024	0-10kPa（Scope of work）	0.24kPa^{-1}	N/A	2Pa	no	no	[1]
Piezoresistive sensors	Au	N/A	0-10kPa（Scope of work）	2.5E-4kPa^{-1}	>0.99	N/A	yes (Independent temperature sensor)	yes	[2]
Pressure capacitive sensors	PDMS	△C/C0 0-10	0-35kPa	2.7kPa^{-1}（0.3–0.6 kPa）	N/A	0.14Pa	no	yes	[3]
Piezoelectric sensors	PZT	-0.1-0.1 V	0-45kPa	0.062kPa^{-1}（0–10 kPa）	N/A	N/A	no	no	[4]
Frictional electrical sensor	Fluorinated ethylene propylene & CNTs	0-10 nA	N/A	0.21μA·kPa^{-1}	0.994	10Pa	no	no	[5]
Frictional electrical sensor	Silicone rubber & paper	0-0.8 V	0–150 kPa	0.89V·kPa^{-1} (0-35kPa)	N/A	43Pa	no	no	[6]

Table S2. The state-of-the-art methods of wearable continuous blood pressure measurement

Sensor type	BP estimation method	Data source – Number of subjects	Generalization	SBP estimation error (mmHg)	DBP estimation error (mmHg)	Ref
Multimodal tactile sensor (Wrist collection)	**MLP inputting pulse wave features, skin temperature and wearing pressure, etc.**	**Own experiments – 18**	**Model generalization across individuals****	**-0.03±5.56 (ME+SD)** **4.43 (MAE)**	**0.05±3.91 (ME+SD)** **3.06 (MAE)**	**This work***
PPG (Fingertip collection)	PWA[7]	Own experiments - 18	Model generalization across individuals	-0.19±8.77 (ME+SD)	0.77±5.26 (ME+SD)	Control experiment in this work
PPG at carotid artery	PWV	Own experiments - 35	Model generalization across individuals	1.15±7.98 (ME+SD)	0.86±6.36 (ME+SD)	8
Wrist frictional electrical pressure sensor	PWA	Own experiments - 20	Model generalization across individuals	0.24±5.27 (ME±SD)	0.54±5.18 (ME±SD)	6
Wrist piezoresistive pressure	PWV	Own experiments -	Model generalization	0.24±5.19 (ME±SD)	0.07±9.66 (ME±SD)	9

sensor+ECG		24	across individuals			
Non-portable multi-lead ECG + PPG finger clip	PWA	MIMIC-II database - 45	Model generalization across individuals	4.43±6.09 (MAE±SAE)	3.32±4.75 (MAE±SAE)	10
PPG finger clip	PWA	MIMIC-III database - 510	Model generalization across individuals	9.43 (MAE)	6.88 (MAE)	11
Single lead ECG on the left and right arms + PPG finger clip	PTT+ PWA	Own experiments - 27	Subject-specific model***	-0.37±5.21 (ME±SD)	-0.08±4.06 (ME±SD)	12
Wrist piezoelectric pressure sensor	Transfer Function	Own experiments - 47	Subject-specific model	-0.89±6.19 (ME±SD)	-0.32±5.28 (ME±SD)	4
Arm and leg single lead ECG + PPG finger clip	PTT+ PWA	Own experiments - 73	Subject-specific model	0.00±3.10 (ME±SD)	0.00±2.20 (ME±SD)	13
Non-portable multi-lead ECG + wrist and ankle PPG	PAT+ PWA	Own experiments - 85	Subject-specific model	1.62±7.76 (ME±SD)	1.49±5.52 (ME±SD)	14
Fingertip multi-wavelength PPG	PTT	Own experiments - 20	Subject-specific model	1.86±2.85 (MAE±SAE)	1.49±1.75 (MAE±SAE)	15
Wrist capacitive pressure sensor	PWA	Own experiments - 7	Subject-specific model	-0.05±2.09 (ME±SD)		16
Wrist piezoelectric pressure sensor + PPG finger clip	PTT	Own experiments - 15	Subject-specific model	2.62±1.92 (MAE+SD)	1.36±1.05 (MAE+SD)	17

PPG finger clip	PWA	MIMIC-II/III database - 15	Subject-specific model	-0.00±6.00 (ME±SD)	0.00±3.30 (ME±SD)	18
Multi Wrist piezoelectric pressure sensor array+ active pressure adaptation unit	PWA	Own experiments - 17	Not stated	−0.05±4.61 (ME±SD)	0.11 ± 3.68 (ME±SD)	19
PPG finger clip	PWA	MIMIC-II database - 1157	Not stated	1.55±5.41 (ME±SD)	-1.25±5.65 (ME±SD)	7
Wrist piezoresistive pressure sensor	PWA	Own experiments - 85	Not stated	0.00±3.06 (ME±SD)	0.10±2.77 (ME±SD)	20

*ME is mean error. SD is standard deviation. MAE is mean absolute error. SAE is standard deviation of absolute error.
** Model generalization across individuals refers to the generalized model is trained and tested across different subjects.
*** Subject-specific model refers to the individual model is trained and tested by the same subject.

References

1. C. Liu, L. Xu, L. Y. Kong, Y. Q. Xu, W. Zhou, Q. P. Qiang, L. L. Tian, W. B. Chen, M. S. Cai, T. C. Lang, T. Han and B. T. Liu, *J. Mater. Chem. C*, 2022, **10**, 13064-13073.
2. Y. S. Oh, J.-H. Kim, Z. Xie, S. Cho, H. Han, S. W. Jeon, M. Park, M. Namkoong, R. Avila, Z. Song, S.-U. Lee, K. Ko, J. Lee, J.-S. Lee, W. G. Min, B.-J. Lee, M. Choi, H. U. Chung, J. Kim, M. Han, J. Koo, Y. S. Choi, S. S. Kwak, S. B. Kim, J. Kim, J. Choi, C.-M. Kang, J. U. Kim, K. Kwon, S. M. Won, J. M. Baek, Y. Lee, S. Y. Kim, W. Lu, A. Vazquez-Guardado, H. Jeong, H. Ryu, G. Lee, K. Kim, S. Kim, M. S. Kim, J. Choi, D. Y. Choi, Q. Yang, H. Zhao, W. Bai, H. Jang, Y. Yu, J. Lim, X. Guo, B. H. Kim, S. Jeon, C. Davies, A. Banks, H. J. Sung, Y. Huang, I. Park and J. A. Rogers, *Nature Communications*, 2021, **12**, 5008.
3. J. C. Yang, J. O. Kim, J. Oh, S. Y. Kwon, J. Y. Sim, D. W. Kim, H. B. Choi and S. Park, *ACS Appl. Mater. Interfaces*, 2019, **11**, 19472-19480.
4. S. W. Min, D. H. Kim, D. J. Joe, B. W. Kim, Y. H. Jung, J. H. Lee, B. Y. Lee, I. Doh, J. H. An, Y. N. Youn, B. Joung, C. D. Yoo, H. S. Ahn and K. J. Lee, *Advanced Materials*, 2023, **35**, 11.
5. Y. S. Fang, Y. J. Zou, J. Xu, G. R. Chen, Y. H. Zhou, W. L. Deng, X. Zhao, M. Roustaei, T. K. Hsiai and J. Chen, *ADVANCED MATERIALS*, 2021, **33**.
6. X. Ran, F. Luo, Z. Lin, Z. Zhu, C. Liu and B. Chen, *Nano Research*, 2022, DOI: 10.1007/s12274-022-4172-2.
7. M. Panwar, A. Gautam, D. Biswas and A. Acharyya, *IEEE SENSORS JOURNAL*, 2020, **20**, 10000-10011.
8. P. M. Nabeel, J. Jayaraj and S. Mohanasankar, *Physiological Measurement*, 2017, **38**, 2122-2140.
9. S. Gong, L. W. Yap, Y. Zhang, J. He, J. Yin, F. Marzbanrad, D. M. Kaye and W. Cheng, *Biosensors and Bioelectronics*, 2022, **205**, 114072.
10. S. Yang, Y. P. Zhang, S. Y. Cho, R. Correia and S. P. Morgan, *Optical and Quantum Electronics*, 2021, **53**, 20.
11. G. Slapnicar, N. Mlakar and M. Lustrek, *Sensors*, 2019, **19**, 17.
12. X.-R. Ding, Y.-T. Zhang, J. Liu, W.-X. Dai and H. K. Tsang, *IEEE Transactions on Biomedical Engineering*, 2015, **63**, 964-972.
13. F. Miao, N. Fu, Y.-T. Zhang, X.-R. Ding, X. Hong, Q. He and Y. Li, *IEEE journal of biomedical and health informatics*, 2017, **21**, 1730-1740.
14. F. Miao, Z.-D. Liu, J.-K. Liu, B. Wen, Q.-Y. He and Y. Li, *IEEE journal of biomedical and health informatics*, 2019, **24**, 79-91.
15. J. Liu, B. P. Yan, Y.-T. Zhang, X.-R. Ding, P. Su and N. Zhao, *IEEE Transactions on Biomedical Engineering*, 2018, **66**, 1514-1525.
16. J. Kim, E. F. Chou, J. Le, S. Wong, M. Chu and M. Khine, *Advanced healthcare materials*, 2019, **8**, 1900109.
17. P. Samartkit, S. Pullteap and O. Bernal, *Measurement*, 2022, **196**, 111211.
18. W.-H. Lin, F. Chen, Y. Geng, N. Ji, P. Fang and G. Li, *BIOMEDICAL SIGNAL PROCESSING AND CONTROL*, 2021, **63**, 102198.
19. J. Li, H. Jia, J. Zhou, X. Huang, L. Xu, S. Jia, Z. Gao, K. Yao, D. Li and B. Zhang, *Nature Communications*, 2023, **14**, 5009.
20. Q. Zhang, L. Shen, P. Liu, P. Xia, J. Li, H. Feng, C. Liu, K. Xing, A. Song and M. Li, *Composites Part B: Engineering*, 2021, **226**, 109365.